Journal of Alloys and Compounds 516 (2012) 33–37

Contents lists available at SciVerse ScienceDirect

Journal of Alloys and Compounds

journal homepage: www.elsevier.com/locate/jallcom

Facile synthesis of Sn–C nanocomposite as an anode material for lithium ion batteries

Jing Wang, Donglin Li*, Xiaoyong Fan, Lei Gou, Jingjing Wang, Yan Li, Xiaoting Lu, Qian Li

Energy Materials & Devices Group, School of Materials Science and Engineering, Chang'an University, Xi'an 710064, China

ARTICLE INFO

Article history:
Received 6 July 2011
Received in revised form
16 November 2011
Accepted 22 November 2011
Available online 30 November 2011

Keywords:
Lithium-ion battery
Anode
Tin
Wet-chemistry
Carbonthermal reduction
Nanocomposite

ABSTRACT

Sn–C nanocomposite is a promising anode material for high performance lithium-ion battery, but suffers from a complex synthesis procedure which hider its practical applicability. We report a simple and cheap synthesis method for Sn–C nanocomposites. By combining wet-chemical and carbonthermal reduction approaches, we are able to produce Sn–C nanocomposite in a simple one-pot synthesis during a successive heating procedure. Gel-derived nanocrystalline SnO_2 is introduced into the precursor to act as a transition-phase for in situ growth of metallic tin nanocrystals. Consequently, this method allows for the fine control of the formation of the tin nanocrystals posterior to the carbonization of carbon sources through carbonthermal reduction of a nanosized SnO_2. The resulting Sn–C nanocomposites deliver a remarkable lithium-ion insertion/extraction performance, such as high capacities of 588 and 367 mA h g^{-1} at 20 mA g^{-1} and 200 mA g^{-1}, respectively.

1. Introduction

There is great interest in developing lithium-ion batteries with higher energy capacity and longer cycle life for wide applications in portable electronic products and electric vehicles. Tin has been suggested as a promising alternative to graphite electrode materials (372 mA h g^{-1}) for high performance lithium-ion battery due to its safety and higher capacity, 993 mA h g^{-1}, in fully lithiated composition $Li_{4.4}Sn$. One major challenge is its large volumetric expansion/contraction upon lithium-ion insertion/extraction. Tin particle begins to crumble away after a few charge–discharge cycles, losing the pathway for lithium ion and electrons transfer. This discontinuity results in a drastic decline of battery performance. Several approaches have been suggested for overcoming this problem. One of the earliest approaches involves alloying with ductile metal which acts as a buffer for volumetric expansion [1–7]. Alternative approach is to use nanosized tin and tin alloy [8–11]. Nanosized particles not only could release mechanical strains within tin particles, but also shortens the diffusion length for lithium ion, which could improve the performance of the battery in high power density. Nanoalloys, however, are still affected by some of disadvantages such as aggregation of active nanoparticles, and high surface reactivity leading to the safety hazard associated with the flammable or explosive tendency of metallic nanopowders. All these problems can be solved by designing and synthesizing the Sn–C nanocomposite in which tin particles dispersed onto an electrochemically inactive carbon matrix that able to buffer the volume expansion assuring the electric conductivity of the material upon cycling [12–25]. In the composite structure, most of the tin particles were encased inside carbon matrix and not easy to aggregate or fall off. And the carbon matrix can accommodate the mechanical stresses/strains of the active phase and acts as an electrical connector with a current collector during the charge–discharge cycles, thus improving the cyclic stability.

Sn–C nanocomposites have been prepared by various approaches, including wet-chemistry [12–18], magnetron sputtering [19], electrospinning [20], electrodeposition [21], and chemical vapor deposition [22,23]. The wet-chemical approach is advantageous to easily doping and controlling over nanoparticle size. Tin nanoparticles could be obtained through the reduction of tin salts using $NaBH_4$ [15–17] or NaH [18] as reduction agents, or the pyrolysis of organic tin precursor at an inert atmosphere [12–14]. Nanosized tin particles are finely dispersed in amorphous carbon matrix, and the Sn–C nanocomposite is capable of delivering full capacity for a cycle life that extends over many hundred of cycles at high discharge rates [12–14]. In some cases mentioned above, in order to prevent from the formation of SnO_2, or to obtain more ideal structure and higher capacity, complex procedures and expensive raw materials are employed, which is noneconomic for practical scale-up synthesis. Furthermore, due to relatively

* Corresponding author.
E-mail address: donglinli@hotmail.com (D. Li).

0925-8388/$ – see front matter © 2011 Elsevier B.V. All rights reserved.
doi:10.1016/j.jallcom.2011.11.097

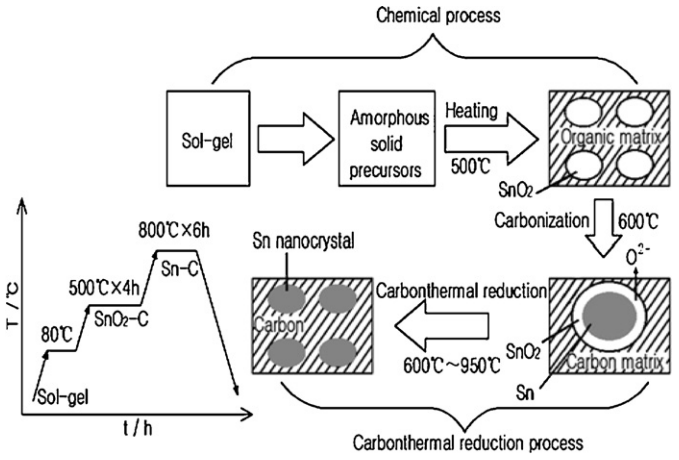

Fig. 1. Schematic diagram of synthesis procedure combined chemical and carbonthermal routes for the Sn–C nanocomposite.

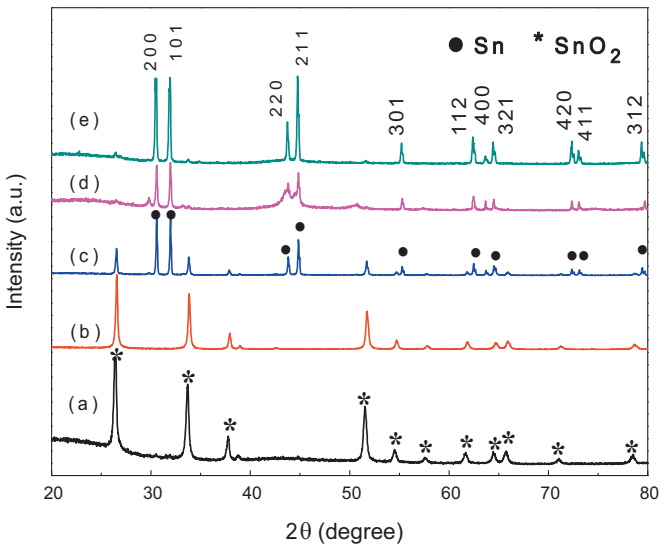

Fig. 2. XRD patterns of the gels annealed at (a) 500 °C, (b) 600 °C, (c) 700 °C, (d) 800 °C, and (e) 950 °C.

low melting point of 220–230 °C [24], tin nanoparticles would be melt prior to the carbonization of organic carbon sources during high temperature thermal treatments. Consequently, the tin could easily coalesce to form liquid droplets in the carbon matrix at carbonization temperatures as high as 500–800 °C, and aggregate easily into a large particle through combining the liquid droplets. Besides these methods, carbonthermal reduction is usually used to synthesize alloy materials. Although Sn–C composites have been synthesized by carbonthermal reduction approach using SnO_2 power as a raw material, tin particles in the composites are on a micrometer scale owning to the aggregation of SnO_2 power [25,26]. Larger tin particles in the Sn–C composites crumble easily after a few charge–discharge cycles. Hence, the development of simple yet reproducible and controllable ways to prepare Sn–C materials exhibiting stable cycleability, especially wet-chemical method, is of importance for its practical application.

In this paper, we report a simple and cheap one-pot synthesis method for preparing Sn–C nanocomposite. Present approach for the synthesis of Sn–C nanocomposite results initially in SnO_2 nanocrystals, followed by reduction of a SnO_2 phase with carbon into the tin nanoparticle in the reduction environment. The metallic tin grows in situ through the reduction of transition-phase SnO_2 nanocrystals by the carbonthermal reaction, posterior to the carbonization of carbon sources due to avoiding the melting of the metallic tin. It is possible to simplify the synthesis procedure in a simple one-pot procedure via combined wet-chemical and carbonthermal reduction approaches, making it possible to finely control over the nanostructure of the Sn–C nanocomposite exhibiting excellent capacity retention with high capacity and rate capability.

2. Experimental

Our synthesis strategy involves a chemical approach for the synthesis Sn–C precursor containing nanocrystalline SnO_2 using $SnCl_4$ as a tin source, and phenol-formaldehyde as carbon source, followed by a carbonthermal reduction for Sn–C nanocomposite, as shown in Fig. 1. The amorphous gel was prepared by a sol–gel method in the chemical process, followed by two successive annealing stages in the temperature range of 500–800 °C (Fig. 1). The annealing procedure involves carbonization of organic carbon sources, crystallization of SnO_2 as a transition phase, and carbonthermal reduction to produce Sn–C nanocomposite in one-pot synthesis during successive heating procedure (see Fig. 1). In a typical synthesis, approximately 3.0 g of phenol and 2.8 g $SnCl_4$ modified by 1.5 mL acetylacetone were dissolved in 1.5 mL formaldehyde solution and 3.0 mL of water. After stirring at 80 °C for 60 min, the brown mixture was aged at 120 °C for 24 h. Then resulting gel was finally annealed in an oven at 500 °C for 4 h and 800 °C for 6 h in a successive heating procedure in flowing argon.

The phase analysis of the synthesized samples was performed using a Rigaku X-ray diffractometer (XRD) with monochromatic Cu K_α radiation. The morphology and microstructure of the synthesized powders were examined with a transmission electron microscope (TEM) at an accelerating voltage of 3000 V.

The electrodes for the electrochemical evaluation were prepared by mixing 80 wt% active materials (Sn–C) powders, 10 wt% carbon black as a conducting agent, and 10 wt% polyvinylidene fluoride (PVDF) dissolved in N-methyl pyrrolidone (NMP) as a binder to form a slurry, followed by coating on a copper foil, pressing, and drying at 120 °C for 3 h under vacuum. The coin cells were assembled in an argon-filled glove-box with the cathodes (Sn–C) thus prepared, lithium foil was used as the counter electrode, 1 M LiPF6 in ethylene carbonate (EC) and dimethyl carbonate (DMC) (1:1 by volume) was used as the electrolyte, and Celgard 2400 was used as separator. The charge–discharge experiments were performed galvanostatically within the voltage range of 0.05–2 V versus Li/Li^+ with LANDCT-2001A testing system.

3. Results and discussion

We initially succeeded in producing the Sn–C nanocomposite with lower tin content. Fig. 2 presents the XRD patterns of the samples with 13.4 wt% tin content annealed at different temperatures. The as-synthesized samples are amorphous before calcinations (not shown). After the samples were annealed at the temperature ranging from 500 to 600 °C, the XRD analysis indicates the formation of SnO_2 nanocrystals with an average size of 36 nm, and no metallic tin phase is detected. When the samples were heated at 600 °C for 6 h, the crystalline phase in the product is composed of both SnO_2 and tin. With further increasing annealing temperature, the intensity of the XRD peaks from SnO_2 gradually diminishes but that from metallic tin becomes stronger (Fig. 2(c)). When annealed at 800 °C, all the reflections could be indexed to a crystalline tin according to JCPDS card No. 04-0673. The size of the tin nanocrystals is estimated to be 28 nm, according to Scherrer equation. The diffraction peak for graphite carbon at about 26.20° is undetectable, suggesting that the carbon is amorphous.

Fig. 3(a) shows the TEM images of the samples annealed at 800 °C, where the dark particles are homogeneously dispersed in the light gray matrix. In order to distinguish tin and carbon phases in Fig. 3(a), the EDS analysis on a large number of particles of the calcined powders was conducted. The results in Fig. 3(b) and (c) confirm that the dark particle marked as EDS1 is tin metal phase, and the light gray matrix marked as EDS2 is carbon. It is noted that a weak oxygen peak is detected in the EDS analysis, whereas the SnO_2 crystalline phase is undetectable in XRD pattern of corresponding sample (Fig. 2(d)). Obviously, a small quantity of SnO_{2-x} phase exists in the tin particles in the sample annealed at 800 °C.

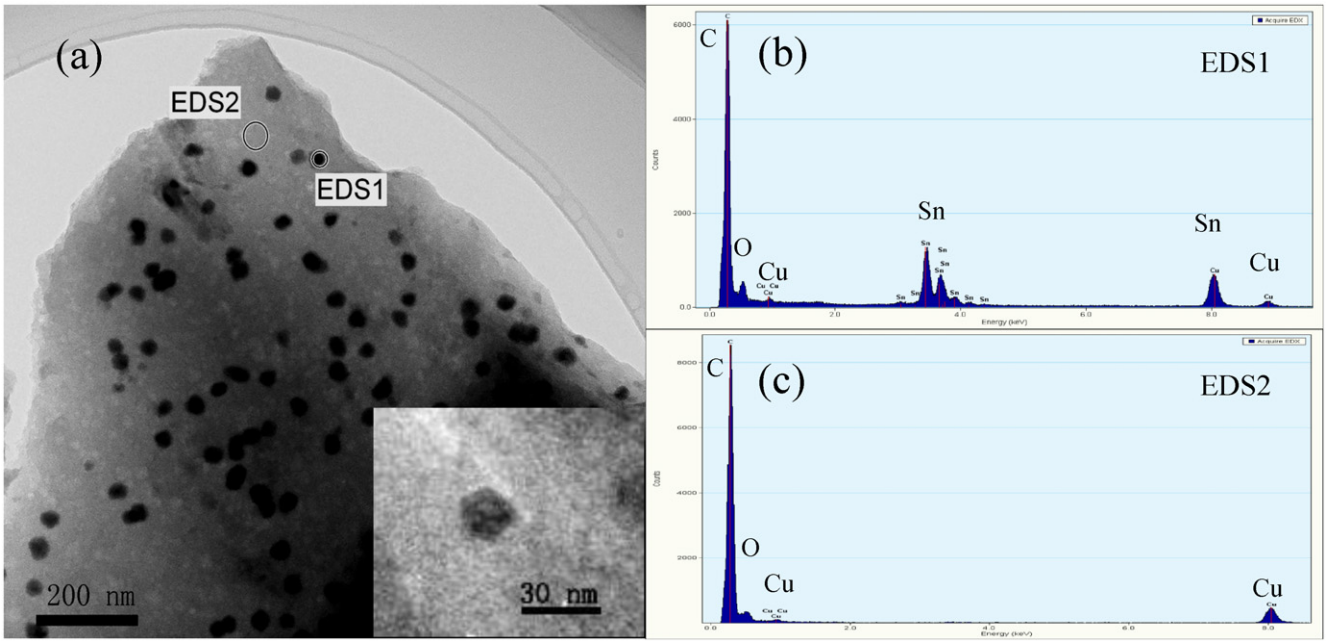

Fig. 3. TEM observation of Sn-C nanocomposite annealed at 800 °C: typical TEM images (a), EDS analyses of (b) dark particles and (c) gray matrix.

The average size of the tin nanoparticle is around 20–30 nm, which is in good agreement with the XRD results. It is worth noting that the morphology of the tin nanoparticle is characterized by a polyhedral shape (Fig. 3(a) inset), indicating that the tin nanoparticles are not yet melted at 800 °C. In contrast, a smoothly spherical shape of the particles, a trace of melted tin droplets, is observed after further annealing at 950 °C (Fig. 4 inset). In this case, the size of the tin nanoparticles increases to 40–100 nm in both the TEM images and the calculation from XRD peak width at half height. Therefore it is believed that the tin nanoparticles are homogeneously dispersed in the carbon matrix by a facile wet-chemical synthesis combined with carbonthermal reduction.

The general formation mechanism of the Sn–C nanocomposite is associated with micro-phase separation of the phenolic resin-based gel which is from the in situ polymerization of the resorcinol with formaldehyde in the presence of $SnCl_4$. The SnO_2–C nanocomposite is obtained after annealing the gel at 500 °C owing to phase separation. With increasing annealing temperature up to 600 °C, the organic carbon source is converted to amorphous carbon. At higher annealing temperatures, the carbonthermal reduction reaction occurs at the interface between SnO_2 nanoparticles and amorphous carbon to produce tin phase under a flowing of inert atmosphere.

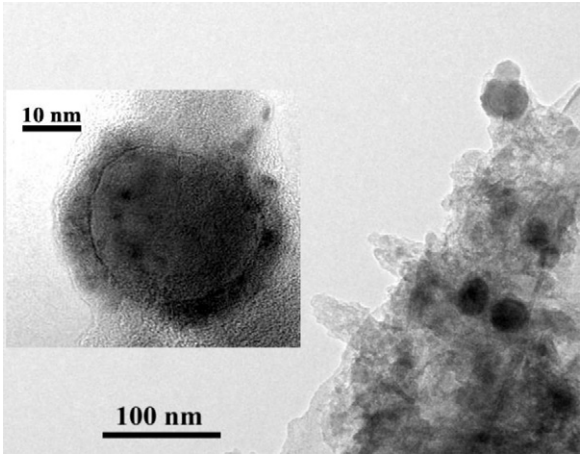

Fig. 4. TEM images of Sn–C nanocomposite annealed at 950 °C.

$$SnO_2 + 2C \rightarrow Sn + 2CO$$

Thus, the existence of SnO_2 phase increases the formation temperature of metallic tin till a complete carbonization of the organic carbon source, avoiding the aggregation of liquid tin nano-droplets. A plausible interpretation of this desired phenomenon is that the tin oxide acts as a skull to prevent tin melts from aggregation [27]. At early period of carbonthermal reaction, the outer layer of SnO_2 particles is poor in oxygen due to the carbonthermal reaction at the boundary between the SnO_2 particles and carbon matrix. As carbonthermal reduction proceeds, the oxygen ions migrate gradually from central bulk to outer layer. Consequently, nucleation of metallic tin phase occurs in the central bulk, and tin phase grows in the core center of SnO_2 particles, producing a core–shell structure in which the core is metallic tin and the shell is SnO_{2-x} (Fig. 1). The SnO_{2-x} shell not only supplies the kinetic condition of carbonthermal reduction but also prevents the tin melts from aggregation. As a result, the tin phase grows in situ from the SnO_2 crystalline phase through carbonthermal reduction reaction above the melting point of tin. When cooling, the melted tin was crystallized in situ into tin nanocrystals.

The charge–discharge profiles and cycle performances of the Sn–C nanocomposite with 13.4 wt% tin content are shown in Fig. 5. In despite of dramatic capacity fade in early several cycles, the Sn–C nanocomposite with 13.4 wt% tin content synthesized at 800 °C exhibits a specific capacity of 240.2 mA h g^{-1} in the 20th cycle with a columbic efficiency of 99%, and still remains 247.6 mA h g^{-1} in the 50th cycle. The voltage plots in Fig. 5(a) for the samples annealed at 800 °C exhibits a characteristic of small nanocrystals similar to amorphous tin. In contrast, the sample annealed at 950 °C shows a specific capacity of 123.1 mA h g^{-1} in the 20th cycle and that of 89.1 mA h g^{-1} in the 50th cycle, which exhibits a dramatic capacity decaying on cycles. The voltage plot in Fig. 5(b) for the materials annealed at 950 °C is characteristic of clear voltage multi-plateaus characteristic of tin crystals with large size [2,28], because the melted tin droplets aggregate into larger tin clusters at 950 °C

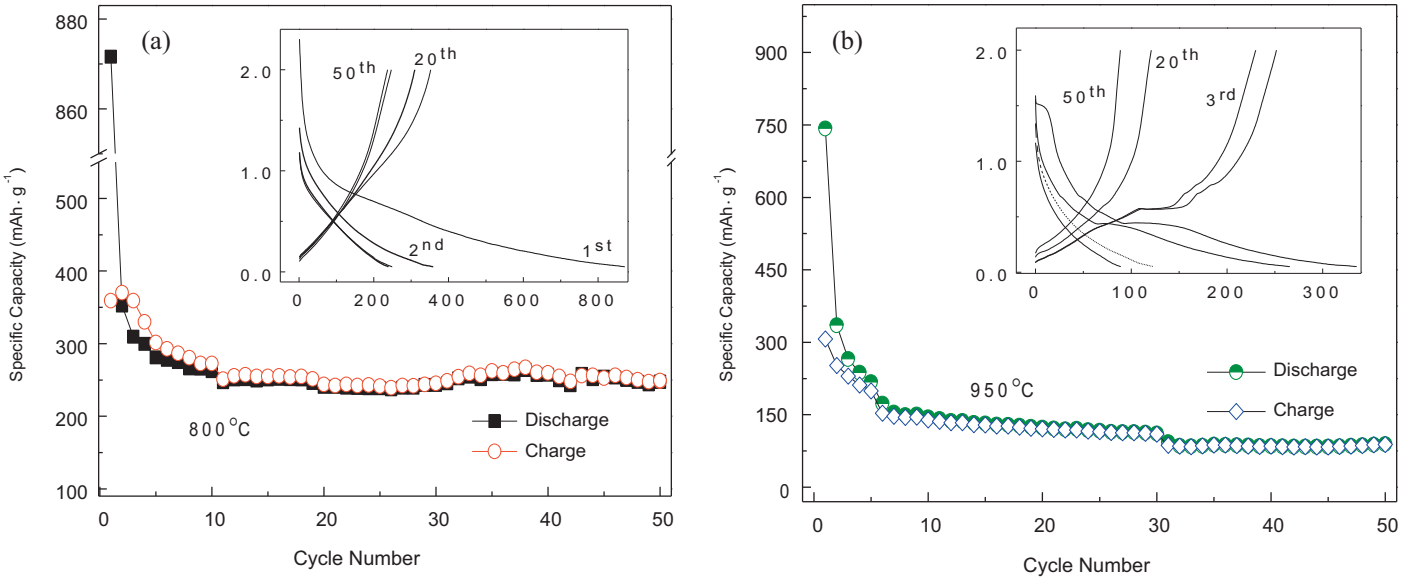

Fig. 5. Galvanostatic charge–discharge profiles and cyclic performance of Sn–C nanocomposite containing 13.4 wt% tin prepared at (a) 800 °C and (b) 950 °C (voltage limits 0.05–2 V versus Li/Li^+).

(Fig. 4). We thus conclude that the uniformly dispersed Sn nanoparticles with an average size of 20–30 nm in the Sn–C nanocomposite show an excellent cycleability during charge–discharge cycles, and the melting of tin could be avoided in our approach by simply controlling annealing temperature.

In order to obtain relatively higher specific capacity, we increased the content of $SnCl_4$ during synthesis products. The XRD and TEM analyses are similar to that of the low tin content. The Sn–C nanocomposite with a composition of about 53.6% tin in weight exhibits a higher reversible specific capacity. The variation of the specific capacity as a function of the discharge rates from 20 to 200 mA g^{-1} is shown in Fig. 6. After early several cycles, the columbic efficiency increases to above 95%, and a stable charge/discharge capacity is maintained in the subsequent cycles. The discharge capacity is about 588.3, 475.8, 419.1, 366.6 mA h g^{-1} at various current densities of 20, 50, 100, and 200 mA g^{-1}, respectively. Even if increasing the current density from 20 to 200 mA g^{-1}, the capacity remains impressively high value of 367 mA h g^{-1} after 200 cycles, thus indicating the merit of nano-structured electrode in the faster discharge. Because the size of the amorphous carbon particles is on the micrometer scale, the rate performance is limited as compared with other tin based materials. If further decreasing the size of the amorphous carbon particles, we anticipate that high rate charge/discharge would be realized.

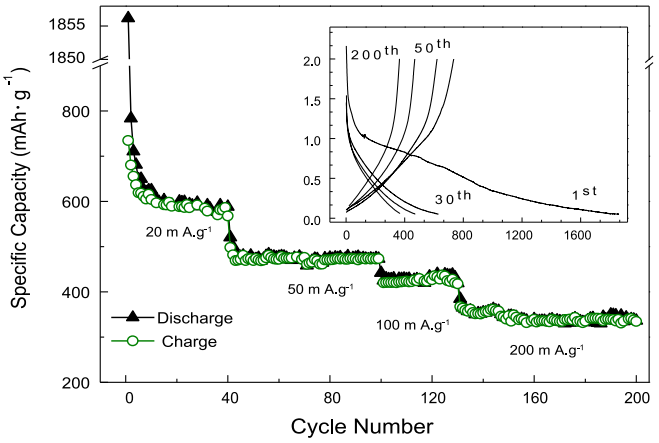

Fig. 6. Galvanostatic charge–discharge profiles and cyclic performance of Sn–C nanocomposite containing 53.6 wt% tin prepared at 800 °C in different current densities (voltage limits 0.05–2 V versus Li/Li^+).

The Sn–C electrode delivers a lithium storage specific capacity of 588.3 mA h g^{-1} in the 40th cycle at 20 mA g^{-1}. The bare carbon obtained by carbonizing organic resorcinol-formaldehyde gels at 800 °C in our work delivers a lithium storage capacity of 125.4 mA h g^{-1} after 40 cycles. Since the maximum specific capacity of the tin component is 993 mA h g^{-1}, the maximum lithium storage specific capacity of the Sn–C nanocomposite in the 40th cycle was estimated as:

$$C_{Sn} \times 53.6\% + C_{ac} \times 46.4\% = 993 \times 0.536 + 125.4 \times 0.464 = 590.434 \text{ mA h g}^{-1}$$

Since the specific capacity of the resultant Sn–C nanocomposite is 588.3 mA h g^{-1} in the 40th cycle, the tin phase is estimated to deliver a capacity of 530.114 mA h g^{-1}, similar to its theoretical capacity of 532.248 (=993 × 53.6%) mA h g^{-1}. The capacity of the Sn–C nanocomposite in our approach is higher than the theoretical specific capacity of graphite anode currently used on the market.

Most of tin-based nano-alloy materials suffer from early columbic inefficiency [12,13,15,17]. The large irreversible specific capacity of the Sn–C nanocomposite is also unavoidable during early several cycles. The irreversible capacity loss may be mainly associated with following reasons. Firstly, the electrolyte reacts with active material surface [12,13,15,17,29,30]. Together with it, the solid electrolyte interface (SEI) at low voltage contributes to the large initial capacity loss during the first charge–discharge cycles. Secondly, the amorphous carbon stores a huge of lithium ions in the first lithium ions insertion, and only a part of lithium ions could be extracted, leading to high irreversible capacity. Because of disordered atomic structure of glassy carbon, a large of inactive lithium ions may be generated in the amorphous carbon. Besides the amorphous carbon structure, the functionalized group of carbon surface derived from the pyrolysis of phenilic resin contributes to inactive lithium ions [31]. Thirdly, the volumetric change in early several cycles may also contribute to dramatic fade of discharge capacity. Although the diameter of tin particles decrease to the nanoscale, the contraction/expansion of the tin alloy is still existing, resulting

in a change of the contacting interface between the tin nanoparticle and carbon matrix within electrodes.

For battery applications, the electrochemical lithium intercalation and extraction capacities are important characteristics of electrode material, which strongly influence the energy density. According to relevant reports, one solution for decreasing irreversible capacity loss is to increases the degree of graphitization as well as to exploring more suitable raw material as carbon precursors that can form a highly crystalline carbon such as a graphitic without functionalized group. The reversible capacity increases with the degree of graphitization, as confirmed by a number of experimental and theoretical studies [32–34]. Except crystallizing carbon phase, more reasonable Sn–C nanostructure such as "Sn core–C shell" structure may be necessary for preventing the harmful interfacial reaction between active phase and electrolyte [17,31].

The above measurements show that we have successfully synthesized the Sn–C nanocomposites with a finely controlled nanostructure by a simple wet-chemical procedure combined with carbonthermal approach. The synthesis approach reported here differs from all previous routes for the Sn–C nanocomposite. In the most of previous works, the Sn precursors were directly reduced to tin metal by using chemical reduction agents. In contract, present approach for the synthesis of Sn–C nanocomposite results initially in SnO_2 nanocrystals, followed by reduction of a SnO_2 phase with carbon into the tin nanoparticle in the reduction environment. As is different from previous work, we introduce the SnO_2 nanocrystals into the precursor, instead of preventing the Sn^{4+} cation from its oxidation. Herein, the SnO_2 nanocrystal is used as a transition-phase for in situ growth of the tin nanocrystal by carbonthermal reduction reaction at a nanoscale. This approach offers several advantages. Firstly, our synthesis condition is not severe, allowing for the use of inert argon gas containing a small amount of air which is much lower-cost than a pure argon. Secondly, the metallic tin grows in situ through the reduction of transition-phase SnO_2 nanocrystals by the carbonthermal reaction, posterior to the carbonization of carbon sources by avoiding the melting of the metallic tin. Because it is easy to finely control the growth and nanostructure of SnO_2, the nanostructure of the Sn–C nanocomposite can be finely controlled. Thirdly, it combines wet-chemical route with conventional carbonthermal reduction reaction into a simple one-pot synthesis process. Therefore, one of important advantages in our work is that the SnO_2 nanocrystal allows us to combine the merits of a chemical route with traditional carbonthermal reduction which is usually used in metallurgy, and thus designing and synthesizing the finely controlled nanostructure of the Sn–C nanocomposite. This type of finely controlled nanocomposite has great potential as node materials in lithium-ion battery.

4. Conclusions

In summary, we have developed a new method for synthesizing the Sn–C nanocomposite via a simple one-pot process which combines the merits of both a chemical route with carbonthermal reduction approaches together. In view of practical use, the present methodology is more economically viable compared to all previous methods, but also more environmentally friendly. The Sn–C nanocomposite exhibits an excellent cyclability, due to avoiding the aggregation and pulverization occurred in tin metal during charge–discharge cycling. Furthermore, this methodology can be easily extended to the preparation of carbon-coated other Li-alloys with multicomponent composition. In the future, in order to decrease the large irreversible capacity during first cycle, one of the possible ways is that the carbon phase should be design to build more reasonable formation such as tin core-crystalline carbon shell structure.

Acknowledgments

This work was supported by National Natural Science Foundation of China (No. 20903016, No. 21073021, and No.21103013), Cultivation Fund of the Key Scientific and Technical Innovation Project, Ministry of Education of China (No. 708084), partially supported by the Fundamental Research Funds for the Central Universities (No. CHD2010ZD008, No. CHD2010JC006, No. CHD2011ZD007, and No. CHD2012ZD001), the Natural Science Foundation of Shaanxi Province (NO. 2010JQ2011).

References

[1] J.O. Besenhard, J. Yang, M. Winter, J. Power Sources 68 (1997) 87.
[2] M. Winter, J.O. Besenhard, Electrochim. Acta 45 (1999) 31.
[3] N. Tamura, M. Fujimoto, M. Kamino, S. Fujitani, Electrochim. Acta 49 (2004) 1949.
[4] I. Amadei, S. Panero, B. Scrosati, G. Cocco, L. Schiffini, J. Power Sources 143 (2005) 227.
[5] K. Nishikawa, K. Dokko, K. Kinoshita, S.W. Woo, K. Kanamura, J. Power Sources 189 (2009) 726.
[6] H.C. Shin, M. Liu, Adv. Funct. Mater. 15 (2005) 582.
[7] X.Y. Fan, F.S. Ke, G.Z. Wei, L. Huang, S.G. Sun, J. Alloy Compd. 476 (2009) 70.
[8] J.G. Ren, X.M. He, L. Wang, W.H. Pu, C.Y. Jiang, C.R. Wan, Electrochim. Acta 52 (2007) 2447.
[9] J. Cho, Electrochim. Acta 54 (2008) 461.
[10] Y.J. Kwon, J. Cho, Chem. Commun. (2008) 1109.
[11] D.G. Kim, H. Kim, H.J. Sohn, T. Kang, J. Power Sources 104 (2002) 221.
[12] G. Derrien, J. Hassoun, S. Panero, B. Scrosati, Adv. Mater. 19 (2007) 2336.
[13] J. Hassoun, G. Derrien, S. Panero, B. Scrosati, Adv. Mater. 20 (2008) 3169.
[14] J. Hassoun, A. Fernicola, M.A. Navarra, S. Panero, B. Scrosati, J. Power Sources 195 (2010) 574.
[15] G.X. Wang, B.W. Wang, X.L. Wang, J. Park, S.X. Dou, H. Ahn, K. Kim, J. Mater. Chem. 19 (2009) 8378.
[16] M. Noh, Y. Kwon, H. Lee, J. Cho, Y. Kim, M.G. Kim, Chem. Mater. 17 (2007) 1926.
[17] W.J. Cui, F. Li, H.J. Liu, C.X. Wang, Y.Y. Xia, J. Mater. Chem. 19 (2009) 7202.
[18] L. Balan, R. Schneider, P. Willmann, D. Billaud, J. Power Sources 161 (2006) 587.
[19] L.Z. Zhao, S.J. Hu, Q. Ru, W.S. Li, X.H. Hou, R.H. Zheng, D.S. Lu, J. Power Sources 184 (2008) 481.
[20] L. Zou, L. Gan, F.Y. Kang, M.X. Wang, W.C. Shen, Z.H. Huang, J. Power Sources 195 (2010) 1216.
[21] J.W. Park, J.Y. Eom, H.S. Kwon, Electrochem. Commun. 11 (2009) 596.
[22] M. Marcinek, L.J. Hardwick, T.J. Richardson, X. Song, R. Kostecki, J. Power Sources 173 (2007) 965.
[23] D. Deng, J.Y. Lee, Angew. Chem. Int. Ed. 48 (2009) 1660.
[24] C.D. Zou, Y.L. Gao, B. Yang, Q.J. Zhai, Trans. Nonferrous Met. Soc. China 20 (2010) 248.
[25] M. Mouyane, J.-M. Ruiz, M. Artus, S. Cassaignon, J.-P. Jolivet, G. Caillon, C. Jordy, K. Driesen, J. Scoyer, L. Stievano, J. Olivier-Fourcade, J.-C. Jumas, J. Power Sources 196 (2011) 6863.
[26] K. Wang, X.M. He, J.G. Ren, C.Y. Jiang, C.R. Wan, Electrochem. Solid-State Lett. 9 (2006) A320.
[27] G.F. Ortiz, P. Lavela, P. Knauth, T. Djenizian, R. Alcántara, J.L. Tirado, J. Electrochem. Soc. 158 (2011) A1094.
[28] I.A. Courtney, J.S. Tse, O Mao, J. Hafner, J.R. Dahn, Phys. Rev. B58 (1998) 15583.
[29] K. Xu, Chem. Rev. 104 (2004) 4303.
[30] G.E. Blomgren, J. Power Sources 81–82 (1999) 112.
[31] J. Ren, X. He, K. Wang, W. Pu, Ionics 16 (2010) 503.
[32] K. Tatsumi, N. Iwashita, H. Sakaebe, H. Shioyama, S. Higuchi, A. Mabuchi, H. Fujimoto, J. Electrochem. Soc. 142 (1995) 716.
[33] A. Mabuchi, K. Tokumitsu, H. Fujimoto, T. Kasuh, J. Electrochem. Soc. 142 (1995) 1041.
[34] H. Shi, J. Barker, M.Y. Saidi, R. Koksbang, J. Electrochem. Soc. 143 (1996) 3466.